MR Imaging of the Substantia Nigra at 7 T Enables Diagnosis of Parkinson Disease[1]

Mirco Cosottini, MD
Daniela Frosini, MD
Ilaria Pesaresi, MD
Mauro Costagli, PhD
Laura Biagi, PhD
Roberto Ceravolo, MD
Ubaldo Bonuccelli, MD
Michela Tosetti, PhD

Purpose: To evaluate the anatomy of the substantia nigra (SN) in healthy subjects by performing 7-T magnetic resonance (MR) imaging of the SN, and to prospectively define the accuracy of 7-T MR imaging in distinguishing Parkinson disease (PD) patients from healthy subjects on an individual basis.

Materials and Methods: The 7-T MR imaging protocol was approved by the Italian Ministry of Health and by the local competent ethics committee. SN anatomy was described ex vivo on a gross brain specimen by using highly resolved proton-density (spin-echo proton density) and gradient-recalled-echo (GRE) images, and in vivo in eight healthy subjects (mean age, 40.1 years) by using GRE three-dimensional multiecho susceptibility-weighted images. After training on appearance of SN in eight healthy subjects, the SN anatomy was evaluated twice by two blinded observers in 13 healthy subjects (mean age, 54.7 years) and in 17 PD patients (mean age, 56.9 years). Deviations from normal SN appearance were described and indicated as abnormal, and both diagnostic accuracy and intra- and interobserver agreement for diagnosis of PD with 7-T MR imaging were calculated.

Results: Three-dimensional multiecho susceptibility-weighted 7-T MR imaging reveals a three-layered organization of the SN allowing readers to distinguish pars compacta ventralis and dorsalis from pars reticulata. The abnormal architecture of the SN allowed a discrimination between PD patients and healthy subjects with sensitivity and specificity of 100% and 96.2% (range, 92.3%–100%), respectively. Intraobserver agreement ($\kappa = 1$) and interobserver agreement ($\kappa = 0.932$) were excellent.

Conclusion: MR imaging at 7-T allows a precise characterization of the SN and visualization of its inner organization. Three-dimensional multiecho susceptibility-weighted images can be used to accurately differentiate healthy subjects from PD patients, which provides a novel diagnostic opportunity.

[1] From the IMAGO7 Foundation, Pisa, Italy (M. Cosottini, M. Costagli); Department of Translational Research and New Surgical and Medical Technologies (M. Cosottini) and Neurology Unit, Department of Clinical and Experimental Medicine (D.F., R.C., U.B.), University of Pisa, Pisa, Italy; Neuroradiology Unit, Department of Diagnostic and Interventional Radiology, Azienda Ospedaliero-Universitaria Pisana (AOUP), Pisa, Italy (I.P.); and Stella Maris Scientific Institute, Pisa, Italy (L.B., M.T.). Received July 23, 2013; revision requested September 27; revision received December 20; accepted December 23; final version accepted December 27. The study is part of an experimental protocol named "Clinical impact of ultra high-field MRI in neurodegenerative diseases diagnosis," RF-2009-1546281, approved and funded by Italian Ministry of Health and cofunded by Health Service of Tuscany. **Address correspondence to** M.C. (e-mail: *mircocosottini@libero.it*).

Parkinson disease (PD) is a common neurodegenerative disease characterized by disabling motor and nonmotor symptoms. The pathologic correlate of nigrostriatal dopaminergic degeneration is the neuronal loss in substantia nigra (SN) pars compacta, particularly in the ventrolateral tier of neurons (1).

Standard magnetic resonance (MR) imaging techniques have a marginal role in the diagnosis and follow-up of PD (2,3), and there is no established MR imaging marker for the diagnosis of PD. T1- and T2-weighted, spin-echo, gradient-recalled-echo (GRE) sequences and segmented inversion-recovery ratio imaging (4) fail to visualize in detail the normal anatomy of the SN, and they are not sufficiently sensitive to the damage caused by nigrostriatal degeneration in PD (5,6). These techniques do not distinguish SN pars compacta from the SN pars reticulata, and therefore correlation with clinical indices of disease severity is difficult, and their employment is of little use in clinical practice (6).

SN-derived biomarkers (eg, relaxometry [7–10], diffusion tensor imaging [11,12], and neuromelanin imaging [13–17]) can be obtained in PD, but they are being evaluated because of interstudy inconsistencies, and they have a limited role in a single-subject evaluation. Currently, none of them is applied in clinical practice (2).

Advances in Knowledge

- MR imaging at 7 T reveals a three-layered organization of the substantia nigra (SN) in both in vivo and ex vivo brainstem.
- MR imaging at 7 T demonstrates in vivo a simple radiologic sign that shows the loss of the intermediate hyperintense SN component that correctly classifies patients with Parkinson disease (PD) with a sensitivity of 100% and specificity of 96.2% (range 92.3%-100%) with excellent intraobserver ($\kappa = 1$) and interobserver ($\kappa = 0.932$) agreement.

Conventional and advanced MR techniques at standard field strength have limitations in the evaluation of SN because both spatial resolution and contrast-to-noise ratio are insufficient to measure the inner structure of SN and the modest quantitative differences induced by the loss of dopaminergic neurons.

MR imaging at 7 T has great potential to provide new insight into neuroanatomy and a wide range of neuropathologic conditions, and could provide new scenarios in the clinical MR application of structural imaging (18). MR imaging at 7 T could be used to increase the spatial resolution by exploiting the higher signal-to-noise ratio to improve the quality of targeted MR images that focus on the brain structures involved in a specific pathologic process (19). In particular, the use of GRE sequences may improve the characterization of nuclei that contain iron and neuromelanin involved in PD (20–23).

We performed an exploratory study to evaluate the anatomy of the SN in healthy subjects by using targeted 7-T MR imaging of the SN, and we prospectively defined the accuracy of 7-T MR imaging to distinguish PD patients from healthy subjects on an individual basis.

Materials and Methods

All patients and control subjects gave their written informed consent to the enrollment and diagnostic procedures on the basis of the adhesion to an experimental protocol that was approved and funded by Italian Ministry of Health and cofunded by the Health Service of Tuscany. The study was approved by the local ethics committee. MR images were obtained from April 2012 to April 2013.

Normal 7-T MR Imaging Anatomy of the SN

The normal 7-T MR imaging anatomy of SN was investigated both ex vivo and in vivo by using a 7-T MR imager (MR950; GE Healthcare, Milwaukee, Wis) equipped with a two-channel transmission and 32-channel receiver head coil (Nova Medical, Wilmington, Mass).

For ex vivo examination of the SN, a gross specimen from a human cadaver of a 67-year-old woman was used. The subject was selected because she had unremarkable neurologic and psychiatric history, she underwent autopsy for death of cardiac origin, and her central nervous system was normal at pathologic examination. The brain specimen, which had been fixed in a 10% aqueous solution of formaldehyde, was removed from formalin and placed in a perfluoropolyether suspension (Fomblin; Solvay-Solexis, Milan, Italy) before it was imaged.

Ex vivo MR imaging acquisitions consisted of proton density–weighted spin-echo two-dimensional GRE and three-dimensional multiecho susceptibility-weighted (SWAN; GE Healthcare) targeted images of the midbrain, acquired in the axial-oblique plane perpendicular to the floor of the fourth ventricle and in the coronal-oblique plane parallel to the floor of the fourth ventricle. The following parameters were used for spin-echo proton density: repetition time msec/echo time msec, 1200/20; number of signals acquired, two; flip angle, 90°; section thickness,

Implication for Patient Care

- The identification of a radiologic marker of the altered SN by using 7-T MR imaging allows an imaging-based early diagnosis of PD.

Published online before print
10.1148/radiol.14131448 **Content code:** NR

Radiology 2014; 271:831–838

Abbreviations:
GRE = gradient recalled echo
PD = Parkinson disease
SN = substantia nigra

Author contributions:
Guarantor of integrity of entire study, M. Cosottini; study concepts/study design or data acquisition or data analysis/interpretation, all authors; manuscript drafting or manuscript revision for important intellectual content, all authors; approval of final version of submitted manuscript, all authors; literature research, M. Cosottini, D.F., I.P., R.C., U.B., M.T.; clinical studies, M. Cosottini, I.P., M. Costagli, L.B., R.C., U.B.; experimental studies, M. Cosottini, D.F., M. Costagli, L.B., M.T.; statistical analysis, M. Cosottini, L.B.; and manuscript editing, all authors

Conflicts of interest are listed at the end of this article.

1 mm; spacing, 1.5 mm; receiver bandwidth, 65.1 kHz; field of view, 10 × 10 cm; in-plane resolution, 190 μm. The following parameters were used for two-dimensional GRE: 240/12.7; two signals acquired; flip angle, 15°; section thickness, 1 mm; spacing, 1.5 mm; receiver bandwidth, 61.0 kHz; field of view, 10 × 10 cm; in-plane resolution, 190 μm. The following parameters were used for the three-dimensional multiecho susceptibility-weighted sequence: 7.5, 15.2, 22.8, 30.3, 37.8/56.5; number of signals acquired, one; section thickness, 1.0 mm; 40 sections; field of view, 16 × 16 cm; receiver bandwidth, 50 kHz; in-plane resolution, 312 μm.

Right-handed healthy subjects (eight healthy subjects [mean age, 40.1 years; age range, 25–62 years]; five women [mean age, 44.4 years; age range, 39–62 years] and three men [mean age, 33 years; age range, 25–40 years]) were consecutively enrolled. We assessed the 7-T MR images of their SNs. They had no personal or family history of psychiatric and neurologic disorders, and their general and neurologic examinations were unremarkable.

In vivo acquisitions were performed by using a three-dimensional multiecho susceptibility-weighted sequence (5.57, 10.7, 15.84, 20.97, 26.1, 31.23, 36.36, 41.5/55.7; number of signals acquired, 0.67; section thickness, 1.2 mm; 18 sections; field of view, 16 × 16 cm; in-plane resolution, 312 μm; receiver bandwidth, 67 kHz), which targeted the midbrain, was oriented in the plane perpendicular to the fourth ventricle floor, and covered 21.6 mm above the pontomesencephalic junction. The imager reconstructed the final output image into a 512 × 512 × 18 matrix by averaging the images obtained for each single echo. The total acquisition time was 242 seconds.

Ex vivo and in vivo 7-T MR targeted images of the midbrain were evaluated by consensus by two experienced neuroradiologists (M.C. and I.P., 21 and 8 years of experience in MR imaging evaluation, respectively) to define the external borders and internal organization of SN. The two observers evaluated SN at the following three levels of the midbrain along the rostrocaudal axis: *(a)* the inferior third of the red nuclei (ie, level I); *(b)* the superior cerebellar pedicle decussation (ie, level II); and *(c)* the inferior colliculi (ie, level III) (Fig 1).

According to the exploratory nature of the work, the normal anatomy of SN at 7 T was assessed by comparing 7-T MR images with neuroanatomic atlases images (24–26).

Pathologic Changes of the SN in PD Patients at 7-T MR Imaging

Nineteen patients with PD (according to clinical criteria for probable PD per the Parkinson's UK Brain Bank [27]) were consecutively enrolled from a tertiary movement disorder center.

Atypical PD disorders (ie, multiple system atrophy, progressive supranuclear palsy, corticobasal degeneration, dementia, and other neurologic or major medical conditions) were considered to be criteria for exclusion. All patients underwent 1.5-T MR imaging to exclude radiologic signs of atypical PD, neoplastic lesions, hydrocephalus, or extensive vascular damage. In newly diagnosed PD patients, levodopa challenge was performed to evaluate acute dopaminergic treatment efficacy, and only patients with a consistent (>30%) improvement in the tapping test were eligible. A 123 iodine fluoropropyl carbomethoxy iodophenyl tropane single-photon-emission computed tomographic scan was performed to confirm nigrostriatal degeneration. Thirteen PD patients were on anti-PD medication at the time of 7-T MR imaging.

Two patients were excluded because their images were severely affected by head motion artifacts. Right-handed PD patients were included in the final analysis (17 patients [mean age, 56.9 years; age range, 38–70 years]; nine women [mean age, 52.2 years; age range, 38–64 years] and eight men [mean age, 61.1 years; age range, 46–70 years]).

Aged-matched (±4 years [tolerated difference for age among PD and healthy subjects]) right-handed healthy subjects (13 healthy subjects [mean age, 54.7 years; age range, 41–66 years]; four women [mean age, 55.2 years; age range, 47–66 years] and nine men [mean age, 54.4 years; age range, 41–64 years]) were enrolled to assess the accuracy of 7-T MR imaging of SN for differentiating PD patients from controls. They had no personal or family history of psychiatric and neurologic disorders, and their general and neurologic examinations were unremarkable.

Demographic and clinical data for healthy subjects and patients are shown in Table 1 (28,29).

The MR imaging protocol for the healthy subjects and PD patients included several different multiparametric acquisitions (18). This contribution focuses on acquisitions obtained by using three-dimensional multiecho susceptibility-weighted sequences with the same parameters evaluation of normal SN anatomy.

After a training on the normal appearance of SN at 7-T MR imaging, two neuroradiologists (M.C. and I.P.) were invited to describe as abnormal any deviation from normal anatomy in three-dimensional GRE (ie, three-dimensional multiecho susceptibility-weighted imaging)-targeted images of SN acquired in PD patients and healthy subjects. SN-targeted three-dimensional multiecho susceptibility-weighted images of PD and healthy subjects were entered into a database and presented in a blinded and randomized manner, which ensured that the readers were unaware of the clinical diagnosis. Readers were asked to give an MR imaging diagnosis according to the abnormal appearance of the SN, and the images of each subject were presented twice after 7 days to calculate intra- and interrater reliability. Subjects were considered to have been affected by PD when at least one level (out of three) of one side of the SN was abnormal. Intra- and interobserver reliability of responses from each reader were cross-tabulated to enable the calculation of agreement and the Cohen κ statistic (30). Demographic data of healthy subjects and PD patients were compared by Student *t* test and χ^2 test. Sensitivity, specificity, and diagnostic accuracy regarding

Figure 1

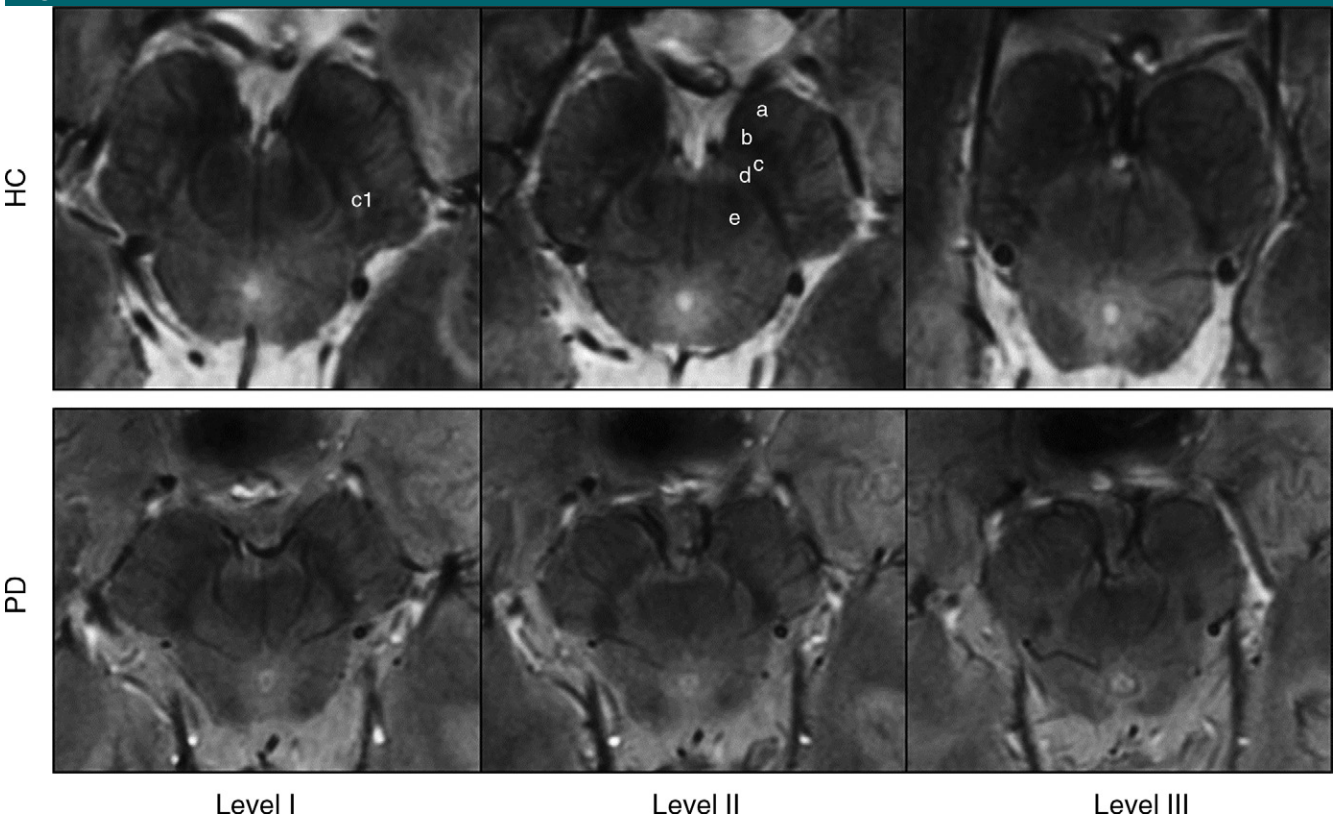

Figure 1: Top row: 7-T three-dimensional multiecho susceptibility-weighted in vivo images of SN in healthy 64-year-old man, located between the crus cerebri *(a)* and the red nucleus. Axial sections perpendicular to the floor of fourth ventricle are obtained at level of the inferior third of the red nucleus (level I), at the level of decussation of superior cerebellar peduncles *(e)* (level II), and at the level of the inferior colliculi (level III). At level I, SN appears as homogeneous hypointense structure in the medial part of the cerebral peduncle, and is laterally constituted by a hyperintense oval area between two hypointense layers *(c1)*. At level II, a trilaminar organization of the SN with a central hyperintense layer *(b)* between two hypointense tiers (*c* and *d*) is detectable. At level III, the dorsal hypointense lamina could be detected as a small residual lateral hypointense area, while the hyperintense layer fades into the isointense cerebral peduncle. Bottom row: 7-T three-dimensional multiecho susceptibility-weighted in vivo images of the SN in PD patients. The loss of normal anatomy of the SN in a 61-year-old man with PD is characterized by the disappearance of the oval-shape bright spot in the lateral part of the SN at level I and by the loss of the hyperintense intermediate layer of the SN at level II. *HC* = healthy subject.

clinical diagnosis were calculated by using statistical software (SPSS v.18; SPSS, Chicago, Ill).

Results

Normal 7-T MR Anatomy of the SN

In vivo three-dimensional multiecho susceptibility-weighted images show the SN as an oval flattened structure that is limited ventrally by the cerebral peduncles and dorsally by the superior cerebellar pedicle decussation and the red nuclei. A homogeneous hypointense region at the upper level (level I) was observed medially by both readers,

Table 1

Demographic and Clinical Data of Healthy Subjects and PD Subjects

Parameter	Healthy Subjects (*n* = 13)	Mean PD Patients ± SD; range (*n* = 17)
No. of men	9	9
No. of women	4	8
Disease duration (mo)	NA	27.2 ± 23.0; 6–96
Hoehn and Yahr	NA	1.7 ± 0.4; 1–2
UPDRS level II	NA	6.9 ± 3.7; 2–13
UPDRS level III	NA	17.8 ± 9.0; 9–37
MMSE	30	29.0 ± 0.3; 29–30

Note.—There were 13 healthy subjects and 17 PD patients. Hoehn and Yahr disease staging (28). MMSE = Mini–Mental State Examination, SD = standard deviation, UPDRS = Unified Parkinson's Disease Rating Scale.

Figure 2

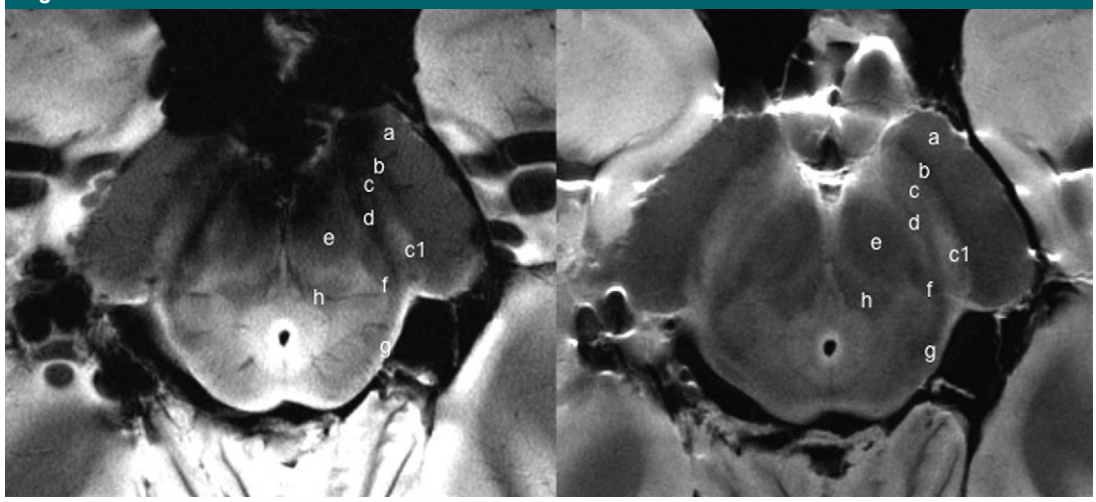

Figure 2: Images show axial spin-echo proton density (on the right) and GRE (on the left) of the SN at level I of an ex vivo brain sample in a 67-year-old woman. There is a triple-layered organization of the SN comparable to that showed in the in vivo images. Ventrally a low-signal-intensity layer *(b)* is attributable to the pars reticulata of the SN. In the middle part of the SN, a hyperintense band *(c)* corresponds to the ventral component of the pars compacta of the SN. The lateral part of this layer shows a high-signal-intensity spot *(c1)* corresponding to the oval shape hyperintensity of the in vivo three-dimensional multiecho susceptibility-weighted images that resemble the nigrosome formation. The dorsal hypointense layer visible on both spin-echo and GRE images *(d)* is referred to the dorsal component of the pars compacta of the SN. *a* = crus cerebri, *e* = brachjum conjunctivum, *f* = medial lemniscus, *g* = lateral lemniscus, *h* = central tegmental tract.

while a small hyperintense area that resembled a bright spot was observed laterally between two hypointense layers. At the longitudinal midlevel (level II), a trilaminar organization was characterized by a central hyperintense layer between two hypointense laminae. At the lower level (level III), the dorsal hypointense lamina was detected as a small residual lateral hypointense area, while the hyperintense layer faded into the isointense cerebral peduncle.

In summary, the two readers agreed in their description of three tiers of signal intensity along the dorsoventrad axis of the midbrain. From back to front, they observed a thin low signal band, followed by a high signal structure, which appeared oval at the upper level (bright spot) and laminar at the midlevel (three layers), and, anteriorly, a large band of signal hypointensity extending anteromedially into the crus cerebri. Both the ventral and dorsal hypointense layers extended along the caudo-rostral and lateromedial direction, and fused laterally at the lower level and medially at the upper level (Fig 1).

Such complex organization of the SN is detectable in even higher detail on ex vivo images (Fig 2). Both readers described a ventral low-signal-intensity layer, an intermediate high-signal-intensity tier and a dorsal low-signal-intensity tier, both on spin-echo proton density (Fig 2, right) and GRE (Fig 2, left) images. Unlike on GRE images, the ventral low-signal-intensity layer on spin-echo proton density images (Fig 2, right) does not extend to the medial part of the crus cerebri that is clearly constituted by white matter fibers.

Pathologic Changes of SN in PD Patients at 7-T MR Imaging

After training on the appearance of SN in healthy subjects, the two readers consensually defined the SN as abnormal if at least one of the following aspects was observed (Fig 1): At the lower level (level III), hypointensity was represented both in the medial and lateral part, and in the middle (level II) and upper levels (level I) the three layered organization and the hyperintense lateral spot were not detectable. The judgment of both readers for each item was reported in Table 2.

For reader 1, abnormal SN in three-dimensional multiecho susceptibility-weighted images was present in 17 of 17 PD patients, while SN was normal in 13 of 13 healthy subjects. Sensitivity, specificity, positive predictive value, and negative predictive value for the diagnosis of PD were each 100%.

For reader 2, SN was judged to be abnormal in 17 of 17 PD patients and normal in 12 of 13 healthy subjects. Sensitivity, specificity, positive predictive value, and negative predictive value for the diagnosis of PD were 100%, 92.3%, 94.4%, and 100%, respectively. κ values were excellent for both intraobserver agreement (κ = 1) and interobserver agreement (κ = 0.932).

Discussion

The main results of the our study are the demonstration of the capability of 7-T MR imaging to depict the borders of the SN and its inner organization, and to reveal simple radiologic signs

Table 2

SN Abnormality

	Healthy Subjects						PD Patients					
Parameter	Level I		Level II		Level III		Level I		Level II		Level III	
Side	R	L	R	L	R	L	R	L	R	L	R	L
Reader 1	0	0	0	0	0	0	17	15	17	15	6	6
Reader 2	1	1	0	0	0	0	17	15	17	15	6	7

Note.—There were 13 healthy subjects and 17 PD patients. The subject was considered affected if one of the following criteria was detectable at least at one level (out of three) of one side (right or left) of the SN. Level I: loss of the hyperintense lateral spot of SN. Level II: loss of the three layers organization of SN. Level III: hypointensity represented both in the medial and lateral part of SN. L = left, R = right.

that show the loss of the three-layer organization and the lateral spot of the SN in PD patients. Those signs allowed us to discriminate with near-perfect accuracy PD subjects from age-matched healthy subjects, which demonstrated a good diagnostic power of 7-T MR imaging in PD.

According to previous pathologic studies (1,31), the SN is a midbrain structure that is anatomically divided into two distinct parts: the inferior and posterior part (SN pars compacta) that contain melanized neurons that project to the striatum and the superior and anterior part (SN pars reticulata), which is low in cells and rich in iron. The internal anatomy of the SN has been differently classified on the basis of the distribution of neurons (1,32–34). According to a classic scheme (1) within the SN pars compacta, two tiers of pigmented neurons are identified, namely the dorsal (SN pars compacta dorsalis) and ventral (SN pars compacta ventralis) tiers oriented anteromedially along the course of the mesencephalon. The anterior and posterior tiers can be further subdivided by using calbindin immunohistochemistry, which reveals zones that are low in calbindin, called nigrosomes, where pigmented neurons reside (33) and PD-related degeneration begins (34).

In our study, 7-T MR targeted images of the midbrain provided a refined depiction of SN internal organization, which allowed for the identification of three tiers of different signal intensity along the posterior-anterior axis of the midbrain in healthy subjects. We believe that the anterior hypointense tier corresponds to the pars reticulata of the SN, and the posterior and intermediate tiers correspond respectively to the dorsal and the ventral components of the SN pars compacta, which is more cellulated and contains dopaminergic neurons (35). In particular, nigrosome 1 is the largest and highly dense cluster of calbindin-negative neurons within the SN pars compacta ventralis (33) and is located in the intermediate and lateral portion of SN pars compacta ventralis, which shows the distribution of the round hyperintense area observed in SN 7-T MR images.

In PD patients, the macroscopic pallor of the SN pars compacta is because of the loss of pigmented neurons.

We argue that the hyperintense signal, visible in the intermediate tier of the SN in healthy subjects, disappeared in PD patients because of either the loss of melanized neurons and/or the increase of iron deposition, which would increase magnetic susceptibility and decrease signal intensity.

Three-dimensional multiecho susceptibility-weighted imaging is a T2*-sensitive sequence in which signal hypointensity may reflect iron accumulation that is considered a PD-related change (1,9,36) that occurs in SN pars compacta. In PD patients, the iron deposits in SN pars compacta reach the level of that in SN pars reticulata, where the iron content is normally twice than in SN pars compacta (37).

Moreover, the loss of the so-called bright spot in the lateral component of the SN pars compacta ventralis in PD corresponds to a recently described (23) disappearance of a pocket-like region inside the lateral portion of the SN that was revealed by a complex surface analysis of the SN obtained at 7 T. In that study (23), Kwon et al reported that PD patients have a volume expansion of the SN, measured by using susceptibility-weighted imaging, and that the larger extent of the signal hypointensity in patients fills in the inflected pocket-like region of the lateral portion of SN that is usually visible in healthy subjects.

Previous 7-T MR imaging studies in patients with PD showed an increasing amount of undulation in the anterior profile of the SN by using GRE images (20). However, this sign appears not to be suitable as a simple method for clinical use because the SN alteration in PD does not mainly involve its reticular component, and because the anterior border of SN pars reticulata in GRE images cannot be precisely identified since it extends beyond its anterior anatomic landmark (6,38).

From a radiologic perspective, to our knowledge this is the first demonstration of a robust MR imaging sign that promptly identifies PD patients with respect to controls. Considering the limited cooperativeness of PD patients, the possibility of reaching a diagnostic result by using a short (242 seconds), single, targeted, three-dimensional, multiecho, susceptibility-weighted sequence with an excellent interobserver agreement is an important goal of 7-T MR imaging. Because at present 7-T MR imaging systems are authorized exclusively for research purpose and not for clinical use, the demonstration of their clinical usefulness and their safety will be the conditions required for their acceptance in the medical community.

The main limitation of our study is that the inner architecture of the SN, identifiable by using 7-T MR imaging, is not confirmed with immunohistochemical methods, and the

distribution of iron, calbindin neurons, and nigrosomal organization within the SN pars compacta may be a matter of debate. As a possible bias regarding definition of the normal anatomy in vivo, we have to consider the younger age of eight healthy subjects that limits the generalization of SN normal anatomy to any age.

Finally, a larger sample of patients would be desirable, but the high diagnostic accuracy of the 7-T MR imaging in PD patients enrolled in this study appears to be a promising result for a future broader clinical application.

Disclosures of Conflicts of Interest: M. Cosottini No relevant conflicts of interest to disclose. **D.F.** No relevant conflicts of interest to disclose. **I.P.** No relevant conflicts of interest to disclose. **M. Costagli** Financial activities related to the present article: received grant money from Fondazione Pisa to install MR system. Financial activities not related to the present article: none to disclose. Other relationships: none to disclose. **L.B.** Financial activities related to the present article: received grant money from Fondazione Pisa to install MR system. Financial activities not related to the present article: none to disclose. Other relationships: none to disclose. **R.C.** No relevant conflicts of interest to disclose. **U.B.** No relevant conflicts of interest to disclose. **M.T.** Financial activities related to the present article: received grant money from Fondazione Pisa to install MR system. Financial activities not related to the present article: none to disclose. Other relationships: none to disclose.

References

1. Fearnley JM, Lees AJ. Ageing and Parkinson's disease: substantia nigra regional selectivity. Brain 1991;114(Pt 5):2283–2301.
2. Lehéricy S, Sharman MA, Dos Santos CL, Paquin R, Gallea C. Magnetic resonance imaging of the substantia nigra in Parkinson's disease. Mov Disord 2012;27(7):822–830.
3. Brooks DJ. Parkinson's disease: diagnosis. Parkinsonism Relat Disord 2012;18(Suppl 1):S31–S33.
4. Hutchinson M, Raff U, Lebedev S. MRI correlates of pathology in parkinsonism: segmented inversion recovery ratio imaging (SIRRIM). Neuroimage 2003;20(3):1899–1902.
5. Minati L, Grisoli M, Carella F, De Simone T, Bruzzone MG, Savoiardo M. Imaging degeneration of the substantia nigra in Parkinson disease with inversion-recovery MR imaging. AJNR Am J Neuroradiol 2007;28(2):309–313.
6. Oikawa H, Sasaki M, Tamakawa Y, Ehara S, Tohyama K. The substantia nigra in Parkinson disease: proton density-weighted spin-echo and fast short inversion time inversion-recovery MR findings. AJNR Am J Neuroradiol 2002;23(10):1747–1756.
7. Ordidge RJ, Gorell JM, Deniau JC, Knight RA, Helpern JA. Assessment of relative brain iron concentrations using T2-weighted and T2*-weighted MRI at 3 Tesla. Magn Reson Med 1994;32(3):335–341.
8. Graham JM, Paley MN, Grünewald RA, Hoggard N, Griffiths PD. Brain iron deposition in Parkinson's disease imaged using the PRIME magnetic resonance sequence. Brain 2000;123(Pt 12):2423–2431.
9. Martin WR, Wieler M, Gee M. Midbrain iron content in early Parkinson disease: a potential biomarker of disease status. Neurology 2008;70(16 Pt 2):1411–1417.
10. Péran P, Cherubini A, Assogna F, et al. Magnetic resonance imaging markers of Parkinson's disease nigrostriatal signature. Brain 2010;133(11):3423–3433.
11. Vaillancourt DE, Spraker MB, Prodoehl J, et al. High-resolution diffusion tensor imaging in the substantia nigra of de novo Parkinson disease. Neurology 2009;72(16):1378–1384.
12. Du G, Lewis MM, Styner M, et al. Combined R2* and diffusion tensor imaging changes in the substantia nigra in Parkinson's disease. Mov Disord 2011;26(9):1627–1632.
13. Menke RA, Jbabdi S, Miller KL, Matthews PM, Zarei M. Connectivity-based segmentation of the substantia nigra in human and its implications in Parkinson's disease. Neuroimage 2010;52(4):1175–1180.
14. Eckert T, Sailer M, Kaufmann J, et al. Differentiation of idiopathic Parkinson's disease, multiple system atrophy, progressive supranuclear palsy, and healthy controls using magnetization transfer imaging. Neuroimage 2004;21(1):229–235.
15. Helms G, Draganski B, Frackowiak R, Ashburner J, Weiskopf N. Improved segmentation of deep brain grey matter structures using magnetization transfer (MT) parameter maps. Neuroimage 2009;47(1):194–198.
16. Sasaki M, Shibata E, Tohyama K, et al. Neuromelanin magnetic resonance imaging of locus ceruleus and substantia nigra in Parkinson's disease. Neuroreport 2006;17(11):1215–1218.
17. Ogisu K, Kudo K, Sasaki M, et al. 3D neuromelanin-sensitive magnetic resonance imaging with semi-automated volume measurement of the substantia nigra pars compacta for diagnosis of Parkinson's disease. Neuroradiology 2013;55(6):719–724.
18. Cho ZH. New brain atlas—Mapping the human brain in vivo with 7.0 T MRI and comparison with postmortem histology: Will these images change modern medicine? Int J Imaging Syst Technol 2008;18(1):2–8.
19. Costagli M, Frosini D, Pesaresi I, et al. Multi-parametric MR imaging of the substantia nigra at 7.0T to investigate Parkinson's Disease [abstr]. In: Proceedings of the Twenty-First Meeting of the International Society for Magnetic Resonance in Medicine. Berkeley, Calif: International Society for Magnetic Resonance in Medicine, 2013.
20. Cho ZH, Oh SH, Kim JM, et al. Direct visualization of Parkinson's disease by in vivo human brain imaging using 7.0T magnetic resonance imaging. Mov Disord 2011;26(4):713–718.
21. Eapen M, Zald DH, Gatenby JC, Ding Z, Gore JC. Using high-resolution MR imaging at 7T to evaluate the anatomy of the midbrain dopaminergic system. AJNR Am J Neuroradiol 2011;32(4):688–694.
22. Lotfipour AK, Wharton S, Schwarz ST, et al. High resolution magnetic susceptibility mapping of the substantia nigra in Parkinson's disease. J Magn Reson Imaging 2012;35(1):48–55.
23. Kwon DH, Kim JM, Oh SH, et al. Seven-Tesla magnetic resonance images of the substantia nigra in Parkinson disease. Ann Neurol 2012;71(2):267–277.
24. Naidich TP, Duvernoy HM, Delman BN, Sorensen AG, Kollias SS, Haacke EM. Duvernoy's atlas of the human brain stem and cerebellum. Vienna, Austria: Springer-Verlag, 2009.
25. Halliday G, Reyes S, Double K. Substantia nigra, ventral tegmental area, and retrorubral fields. In: Mai JK, Paxinos G eds. The human nervous system. 3rd ed. London: Elsevier Academic Press, 2012; 439–455.
26. Nieuwenhuys R, Voogd J, van Huijzen C. The human central nervous system: a synopsis and atlas. 4th rev ed. New York, NY: Springer, 2007.
27. Gibb WR, Lees AJ. The relevance of the Lewy body to the pathogenesis of idiopathic Parkinson's disease. J Neurol Neurosurg Psychiatry 1988;51(6):745–752.
28. Hoehn MM, Yahr MD. Parkinsonism: onset, progression and mortality. Neurology 1967;17(5):427–442.

29. Fahn S, Elton RL; members of the UPDRS Development Committee. Unified Parkinson's disease rating scale. In: Fahn D, Marsden CD, Calne D, Goldstein M, eds. Recent developments in Parkinson's disease. Vol 2. Florham Park, NJ: Macmillan Healthcare Information, 1987.

30. Landis JR, Koch GG. The measurement of observer agreement for categorical data. Biometrics 1977;33(1):159–174.

31. Massey LA, Yousry TA. Anatomy of the substantia nigra and subthalamic nucleus on MR imaging. Neuroimaging Clin N Am 2010; 20(1):7–27.

32. Hassler R. Zur Normalanatomie der Substantia nigra. Versuch einer architektonischen Gliederung. J Psychol Neurol 1937;48(1-2):1–55.

33. Damier P, Hirsch EC, Agid Y, Graybiel AM. The substantia nigra of the human brain. I. Nigrosomes and the nigral matrix, a compartmental organization based on calbindin D(28K) immunohistochemistry. Brain 1999; 122(Pt 8):1421–1436.

34. Damier P, Hirsch EC, Agid Y, Graybiel AM. The substantia nigra of the human brain. II. Patterns of loss of dopamine-containing neurons in Parkinson's disease. Brain 1999;122(Pt 8):1437–1448.

35. Gibb WR, Lees AJ. Anatomy, pigmentation, ventral and dorsal subpopulations of the substantia nigra, and differential cell death in Parkinson's disease. J Neurol Neurosurg Psychiatry 1991;54(5):388–396.

36. Gorell JM, Ordidge RJ, Brown GG, Deniau JC, Buderer NM, Helpern JA. Increased iron-related MRI contrast in the substantia nigra in Parkinson's disease. Neurology 1995;45(6): 1138–1143.

37. Sofic E, Paulus W, Jellinger K, Riederer P, Youdim MB. Selective increase of iron in substantia nigra zona compacta of parkinsonian brains. J Neurochem 1991;56(3): 978–982.

38. Rutledge JN, Hilal SK, Silver AJ, Defendini R, Fahn S. Study of movement disorders and brain iron by MR. AJR Am J Roentgenol 1987;149(2):365–379.